EXPERIMENTS OF CONTROLLABLE FRICTION DAMPER USING PIEZOELECTRIC ACTUATORS FOR SEMI-ACTIVE SEISMIC ISOLATION SYSTEM

Eiji SATO[1] and Takafumi FUJITA[2]

ABSTRACT: A semi-active seismic isolation system using a controllable friction damper was developed to decrease relative displacement between ground and a superstructure. However, if the controller of the controllable friction damper breaks down when a great earthquake occurs, it cannot demonstrate its full performance. In this study, a new controllable friction damper using dependable piezoelectric actuators is proposed to slove this problem. This damper has a fail-safe mechanism enabling the system to demonstrate damping effect in case of malfunctions. This paper outlines the results of the characterization experiments of the controllable friction damper. It also reports the simulation results for the seismic isolation effects and the relative displacement reduction effects of semi-active seismic isolation system using the controllable friction damper.

Key Words: *semi-active seismic isolation system, controllable friction damper, piezoelectric actuator*

INTRODUCTION

In order to decrease response acceleration of superstructures during an earthquake, several base-isolated buildings have been constructed using passive isolation systems (Fujita 1991a). However, there is a trade-off problem that large relative displacements are inevitable in the passive seismic isolation system to decrease the response acceleration of the superstructures.

To solve this trade-off problem, a semi-active seismic isolation system using a controllable friction damper was developed, in which the damping force was controlled by varying the pressure between the friction elements (Fujita 1991b, Fujita 1992). However, if the actuator which presses the friction element breaks down, the damping force cannot be generated at all.

To solve this problem, a new controllable friction damper with fail-safe mechanism was produced. In addition, to make the mechanism simple, piezoelectric actuators which are dependable and can generate large force were used. Several experiments were conducted to obtain characteristics of this controllable friction damper. From the results of the characterization experiments, a numerical model of the controllable friction damper was developed. Then, the numerical model of the controllable friction damper was used for the response analysis of the semi-active isolation system. This paper reports the results of the experiments and analyses.

[1] Cooperative Research Fellow
[2] Professor

CONTROLLABLE FRICTION DAMPER

A controllable friction damper of the conventional system (hereafter referred as "holding type controllable friction damper") generates friction force by pressing a friction element with an actuator. The mechanism of the holding type controllable friction damper is shown in Figure 1.

This damper cannot generate damping force in case that the power source of the system is cut off due to of a large earthquake. To solve this problem, a controllable friction damper with fail-safe mechanism is proposed. Damping force in the proposed damper (hereafter referred as "releasing type controllable friction damper") can be generated in such cases. The mechanism of the releasing type controllable friction damper is shown in Figure 2. At the initial state, the friction materials are pressed. Once an earthquake occurs, the actuator force is applied to reduce the friction by releasing the pressure between the friction elements. The friction force can be changed with controlling the actuator force. Even if the controller and the actuator of this damper break down and the actuator force $p(t)$ becomes zero, the damping force can be generated by the initial pressure p_0.

The plan and sections of the releasing type controllable friction damper produced for experimental use is shown in Figure 3. The initial pressure p_0 is generated by two press bolts on top and bottom of the center. Strain gages which are attached on the two press bolts are calibrated by a tension test beforehand. They are used as load cells to measure the pressure between the friction elements. In total, eight piezoelectric actuators are set up in four locations in both sides of these press bolts. Therefore, the releasing force is generated with the piezoelectric actuators.

The piezoelectric actuator is shown in Figure 4. The size, the maximum driving voltage, the range for displacement and the range for generation force of the piezoelectric actuator are $25\times25\times36$ mm, 100V, 20 μ m and 20kN, respectively. The relationship between the generation force and the displacement is shown in Figure 5 (Shimazaki 1996). The pre-load of the piezoelectric actuators is adjusted with the pre-load bolts. As a result, the generation force and displacement of the piezoelectric actuator are adjusted.

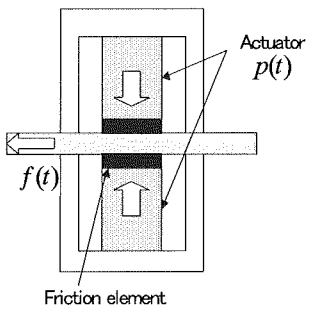

Figure 1. Holding type controllable friction damper

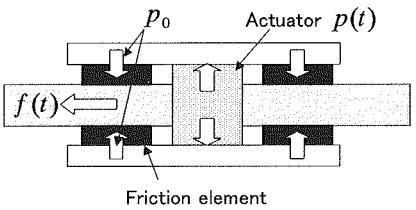

Figure 2. Releasing type controllable friction damper

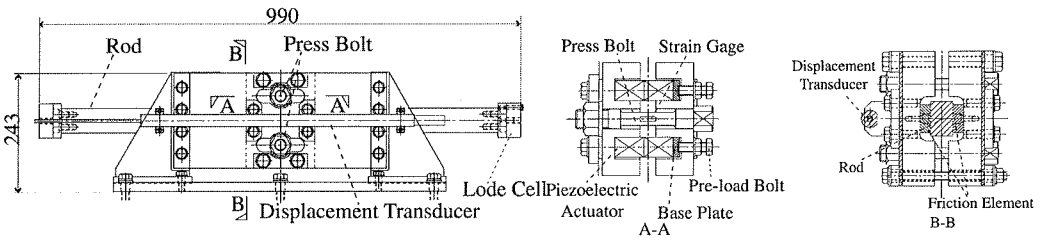

Figure 3. Plan and sections of the releasing type construction of controllable friction damper

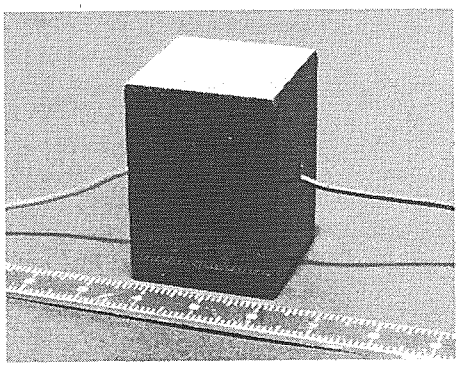

Figure 4. Piezoelectric actuator

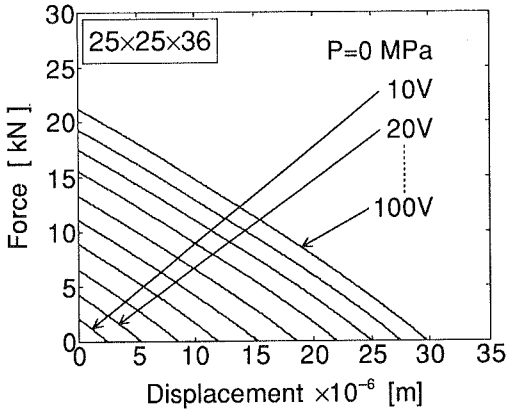

Figure 5. Relationship of generation force and displacement

CHARACTERIZATION EXPERIMENT

Experimental apparatus and instrumentation

The experiment layout is shown in Figure 6 and the experimental apparatus and the instrumentation system are shown in Figure 7. The friction damper is excited with the hydraulic actuator set in one side of the rod. The friction force is measured with the load cell set between the rod and hydraulic actuator. The displacement of the friction damper is measured with a displacement transducer. The releasing force by piezoelectric actuators is calculated from the strain of the press bolts. The driving voltage to the piezoelectric actuators is calculated from the command voltage inputed to the piezo driver.

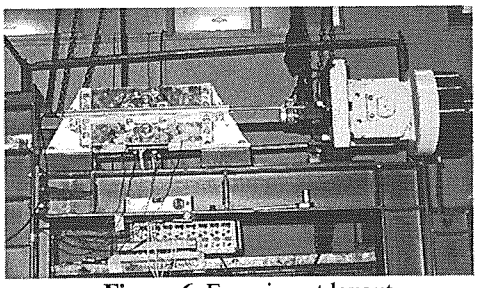

Figure 6. Experiment layout

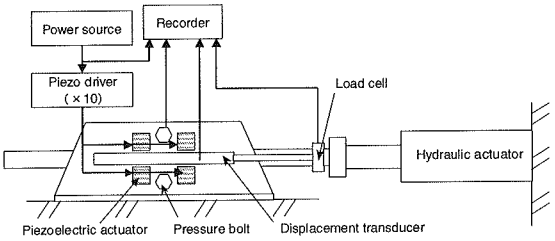

Figure 7. Experiment apparatus and instrumentation system

Experimental condition

The experimental conditions are shown in Table 1. All the excitation waves were set as a triangular wave, and the amplitude was fixed to 15cm which was the maximum displacement of the friction damper. Four different velocities were used to examine the velocity dependence of the friction force.

Table 1. Experiment condition

Excitation Wave	Amplitude [cm]	Velocity [cm/s]	Voltage applied to Piezo [V]	
Triangular Wave	15	6,12, 18,24	Constant	0,25,50, 75,100
			Ramp	100-0
			Sine wave	100p-p (1Hz, 2Hz)

Velocity-dependent test

Figure 8 shows the friction force of the damper at each excitation velocity, when zero volt was applied to the piezoelectric actuators. The figure indicates that the friction force did not depend on the sliding velocity and was constant. Twenty five V, 50V, and 100V were applied to the piezoelectric actuators, and the pressure between the friction elements changed. Figures 9, 10, and 11 show the results. Similarly, the friction force did not depend on the sliding velocity and was constant.

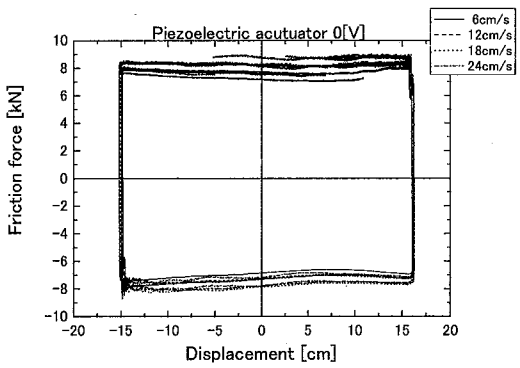

Figure 8. Result of velocity dependence test (0 V was applied)

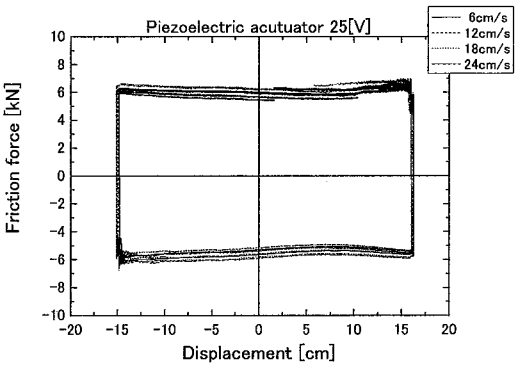

Figure 9. Result of velocity dependence test (25 V was applied)

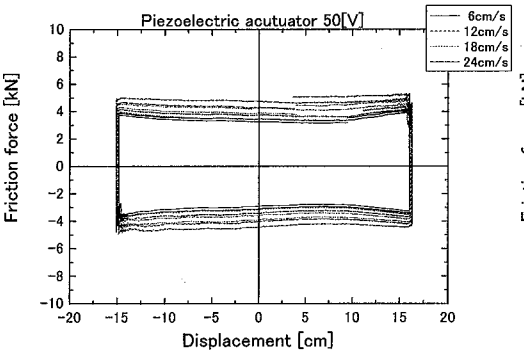

Figure 10. Result of velocity dependence test (50 V was applied)

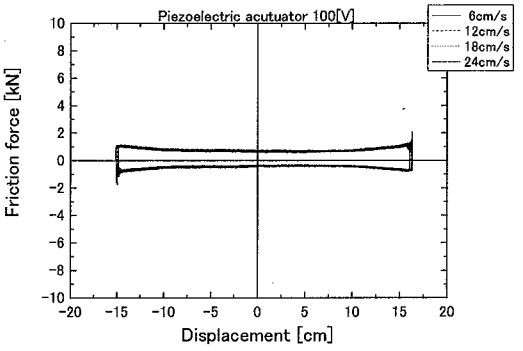

Figure 11. Result of velocity dependence test (100 V was applied)

Input voltage and the friction force

Figure 12 shows the relationship between the applied voltage to the piezoelectric actuators and the friction force of the damper when the applied voltage to the piezoelectric actuators was changed from

zero to 100V in the sinusoidal wave. Though hystereses behavior existed in the relationship between the applied voltage to the piezoelectric actuator and the friction force of the damper, this relationship was approximated to a linear function for simplification. The approximated linear function was as follows:

$$f(t) = 6.17 - 0.0528E(t) \tag{1}$$

where

$f(t)$: Friction force of the controllable friction damper of releasing type [kN]

$E(t)$: Applied voltage to the piezoelectric actuators [V]

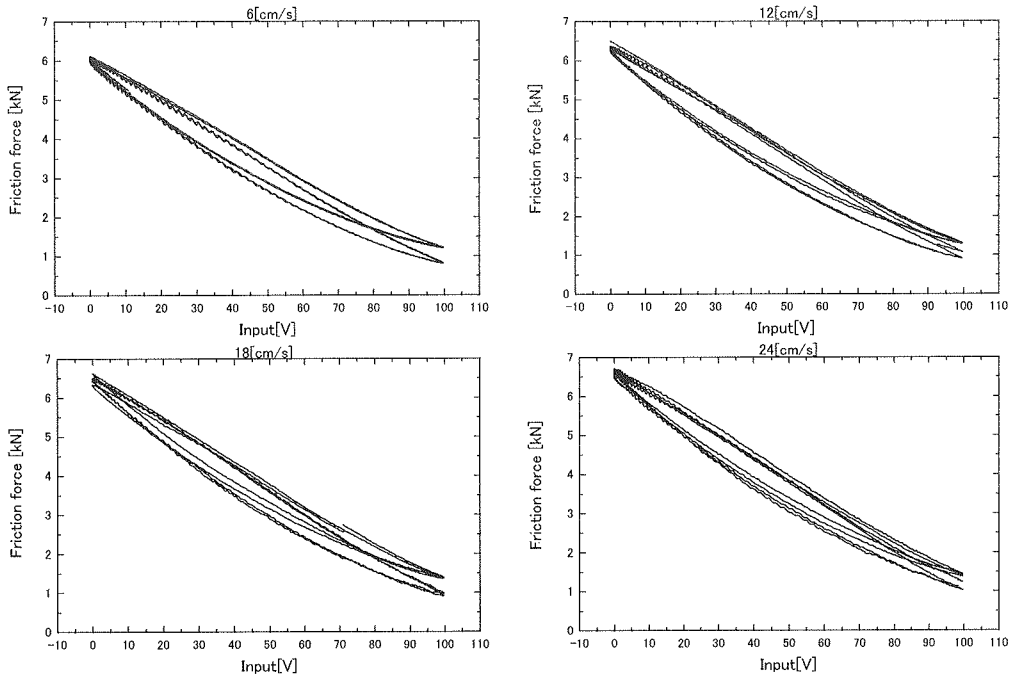

Figure 12. Applied voltage and friction force relationship

SIMULATION OF SEISMIC ISOLATION SYSTEM USING CONTROLLABLE FRICTION DAMPER

Analysis model

The seismic isolation system using the controllable friction damper is modeled as a single degree of freedom system, as shown in Figure 13. Equations of motion of the model are expressed in two phases, as shown below, considering changeover of static/dynamic friction due to presence or absence of sliding at the friction damper.

(1) Phase I : No sliding at friction damper

$$\begin{cases} x = const. \\ \dot{x} = 0 \\ \ddot{x} = 0 \end{cases} \tag{2}$$

(2) Phase II : Sliding at friction damper

$$\ddot{x} + 2\zeta\omega\dot{x} + \omega^2 x + \mathrm{sgn}(\dot{x})F = -\ddot{z} \tag{3}$$

And the changeover criteria between Phase I and Phase II are as follows:
1) From Phase I to Phase II

$$|kx + m\ddot{z}| > f \tag{4}$$

2) From Phase II to Phase I

$$\dot{x} = 0 \quad \text{and} \quad |m\ddot{x}| < 2f \tag{5}$$

where

$$\zeta = \frac{c}{2\sqrt{mk}} \ , \ \omega = \sqrt{\frac{k}{m}} \ , \ F = \frac{f}{m}$$

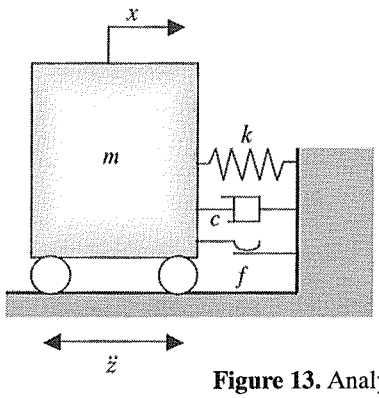

x : Relative displacement of the superstructure to the ground
m : Mass of the superstructure
k : Spring constant of the passive isolation device
c : Damping coefficient of the passive isolation device
f : Friction force

Figure 13. Analysis model

Linear quadratic optimum regulator theory

The optimal generation force is obtained by using linear quadratic optimum regulator theory (LQ). Then, the optimal friction force is derived from this optimal generation force and the condition of a semi-active control. A performance function is defined as follows:

$$J = \int_0^\infty \left\{\alpha(\ddot{x} + \ddot{z})^2 + \beta x^2 + \gamma u^2\right\} dt \tag{6}$$

where

α, β, γ : Weighting coefficients

Here, the equation of motion of the building model Equation (3) is transformed into the following equation of state:

$$X = AX + Bu + d\ddot{z} \tag{7}$$

where

$$\left(X=[x,\dot{x}]^T\right), A=\begin{bmatrix}0 & 1\\ -\omega^2 & -2\zeta\omega\end{bmatrix}, B=\begin{bmatrix}0\\ -1\end{bmatrix}, d=\begin{bmatrix}0\\ -1\end{bmatrix}$$

The next equation is obtained by substituting Equation (7) for Equation (6).

$$J=\int_0^\infty \left(X^TQX+2X^TSU+U^TRU\right)dt \tag{8}$$

Optimal regulator problem is solved from Equation (8). The optimal feedback vector F_b and the optimal control input u^* are obtained as follow:

$$F_b=R^{-1}(S^T+B^TP) \tag{9}$$

$$u^*=-F_bX \tag{10}$$

Since friction force cannot be generated in the same direction as the velocity of superstructure, the condition of a semi-active control is shown as follows:

$$f=\begin{cases}u^* & (u^*\cdot\dot{x}>0)\\ 0 & (u^*\cdot\dot{x}<0)\end{cases} \tag{11}$$

The optimal friction force is derived from Equation (10) and Equation (11).

The seismic isolation effect and the displacement reduction performance by the weighting coefficients α, β of the performance function Equation (6) were examined. The mass of the model was 6,000 kg, and the natural period and the damping ratio of the seismic isolation system were 3 sec and 2 %, respectively. The input waves were EL Centro NS (1940, Imperial Valley Earthquake), JMA NS (1995 Hyogoken-Nanbu Earthquake), Hachinohe NS (1968 Tokachi-Oki Earthquake) and Taft EW (1952 Arvin-Tahachapi Earthquake). The velocity level of the input waves was set to 25 cm/s for each wave. Figures 14,15,16 and 17 show the maximum response accelerations of superstructure and the maximum relative displacements between the superstructure and the ground when the weighting coefficients α and β were changed. For comparison, the flat surface in these figures show the results of a passive seismic isolation system with ideal linear damping ratio of 20%.

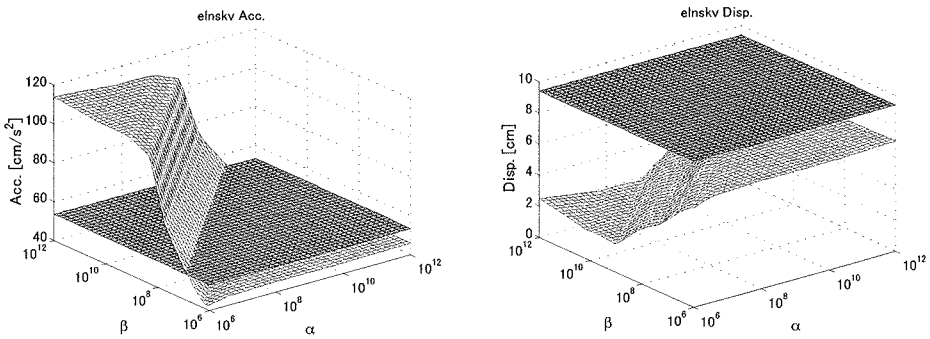

(a) Maximum response accelerations (b) Maximum relative displacement

Figure 14. Maximum response results (EL Centro NS)

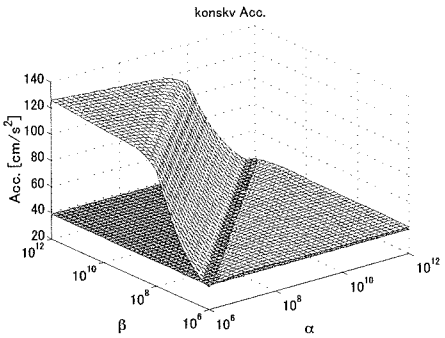

(a) Maximum response accelerations (b) Maximum relative displacement

Figure 15. Maximum response results (JMA NS)

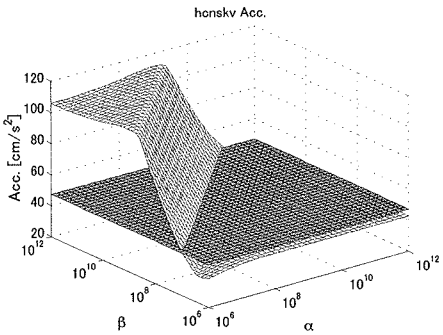

(a) Maximum response accelerations (b) Maximum relative displacement

Figure 16. Maximum response results (Hachinohe NS)

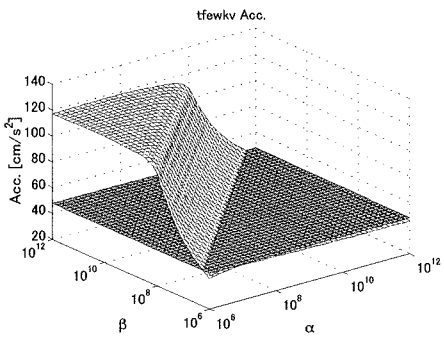

(a) Maximum response accelerations (b) Maximum relative displacement

Figure 17. Maximum response results (Taft EW)

From these results, it is found that the displacement reduction performance improved with semi-active seismic isolation using the releasing type controllable friction damper for all values of the weighting coefficients α and β, compared with the passive seismic isolation system. Though the difference is seen by the seismic wave, the area where the seismic isolation effects improved more than the passive seismic isolation system exists. By comparing with the passive seismic isolation results, the weighting coefficients were selected in the following cases:

1) The response acceleration is almost in the same level and the displacement is smaller. (displacement reduction)
2) Both the response acceleration and relative displacement are smaller (acceleration and displacement reduction)

Figures 18,19,20 and 21 show the results of the analyses by these weighting coefficients when the velocity level of the input waves was set to 25, 50,75 and 100 cm/s for each wave.

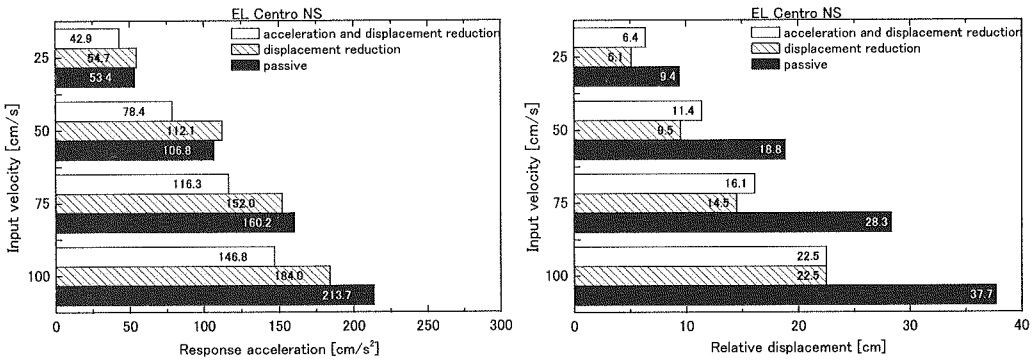

(a) Maximum response accelerations (b) Maximum relative displacement

Figure 18. Response results by selected weighting coefficients (EL Centro NS)

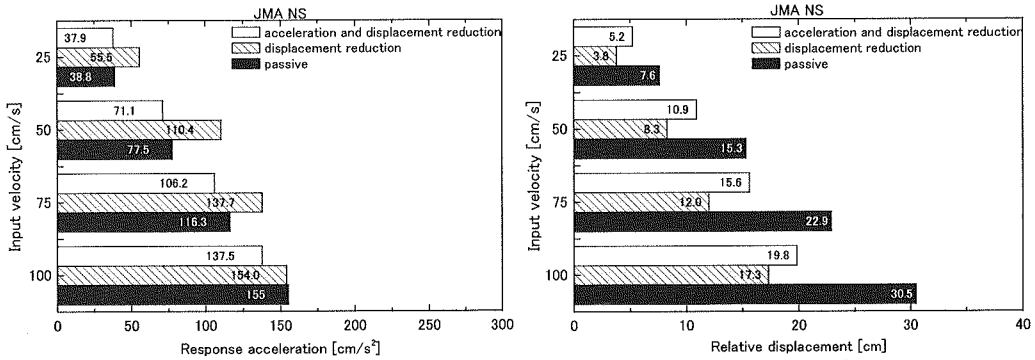

(a) Maximum response accelerations (b) Maximum relative displacement

Figure 19. Response results by selected weighting coefficients (JMA NS)

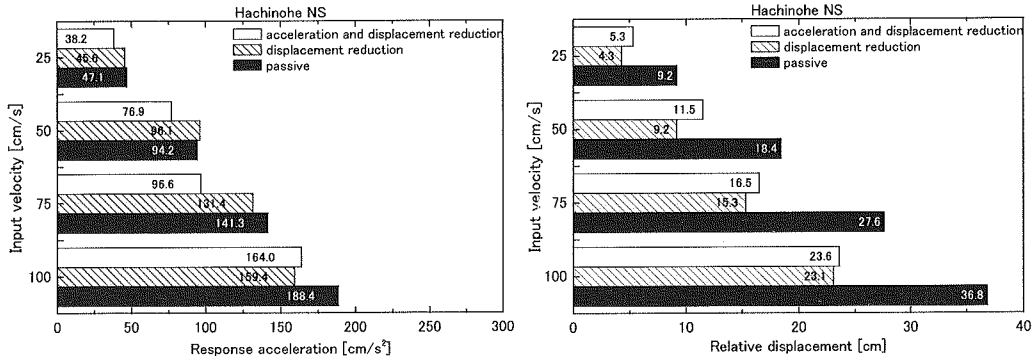

(a) Maximum response accelerations (b) Maximum relative displacement

Figure 20. Response results by selected weighting coefficients (Hachinohe NS)

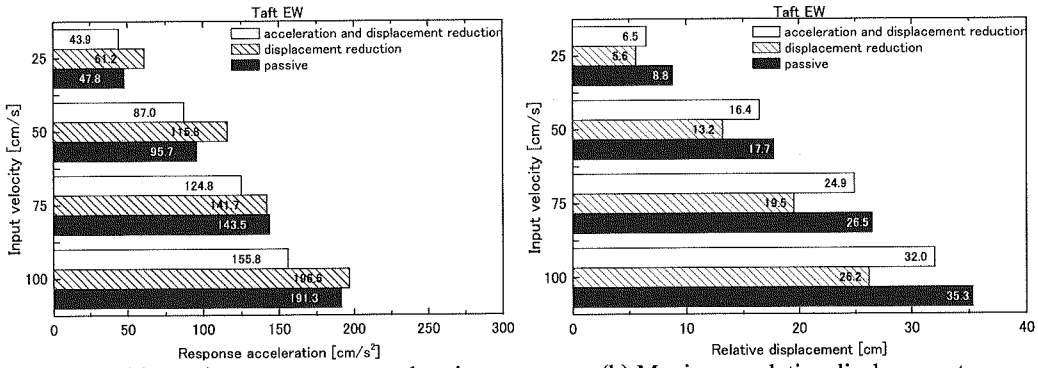

(a) Maximum response accelerations (b) Maximum relative displacement

Figure 21. Response results by selected weighting coefficients (Taft EW)

Instantaneous optimal control

When the releasing type controllable friction damper is used, the equation of motion of the seismic isolation system is nonlinear. Instantaneous Optimal Control algorithm (hereafter referred as "IOC"), which is effective on a nonlinear system, is used to obtain optimal piezoelectric actuator force $p(t)$. As a performance function of IOC, the following function $J(t)$ is defined:

$$J(t) = q_v \dot{x}^2(t) + q_d x^2(t) + q_f F^2(t) + p^2(t) \tag{12}$$

where

$q_v \geq 0$, $q_d \geq 0$, $q_f \geq 0$: Weighting coefficients

The optimal piezoelectric actuator force $p^*(t)$ to minimize the performance function $J(t)$ is obtained as follows:

$$\begin{aligned} p^*(t) = & \frac{q_f \mu^2}{m^2 + q_f \mu^2} p_o \\ & - \frac{q_v m \mu \Delta t \, \mathrm{sgn}(\dot{x}(t))}{2\left(m^2 + q_f \mu^2\right)\left(1 + \frac{\Delta t^2}{6}\omega^2 + \Delta t \zeta \omega\right)} \dot{x}(t) \\ & - \frac{q_d m \mu \Delta t^2 \, \mathrm{sgn}(\dot{x}(t))}{6\left(m^2 + q_f \mu^2\right)\left(1 + \frac{\Delta t^2}{6}\omega^2 + \Delta t \zeta \omega\right)} x(t) \end{aligned} \tag{13}$$

where

μ : Friction coefficient

Δt : Sampling time

The seismic isolation effect and the displacement reduction performance by the weighting coefficients q_v, q_d, q_f of the performance function Equation (12) for IOC were examined. The analytical condition was the same as the case of LQ.

First of all, the weighting coefficient q_f was examined. The optimal piezoelectric actuator force is

shown by Equation (13), and the right initial term of Equation (13) becomes a constant which does not depend on the amount of feedback. Moreover, this term shows the initial releasing force when the earthquake occurs, and this initial releasing force is only decided by the weighting coefficient q_f. The weighting coefficient q_f was set so that the friction damper could begin the slip when the acceleration of earthquake ground motion became 25cm/s^2 or more, because an excellent result was obtained.

Next, the weighting coefficients q_v and q_d were examined. Figures 22, 23, 24 and 25 show the maximum response accelerations of superstructure and the maximum relative displacements between the superstructure and the ground, when above-mentioned q_f was used and the weighting coefficients q_v and q_d were changed. For comparison, the results of the passive seismic isolation system with ideal linear damping of 20% are shown in these figures.

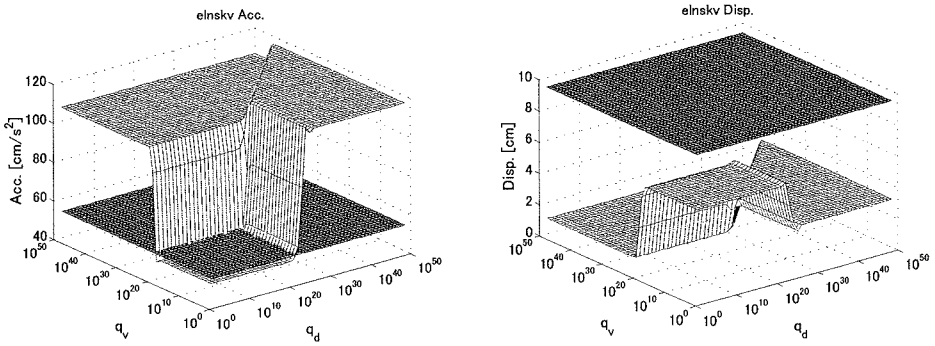

(a) Maximum response accelerations (b) Maximum relative displacement

Figure 22. Maximum response results (EL Centro NS)

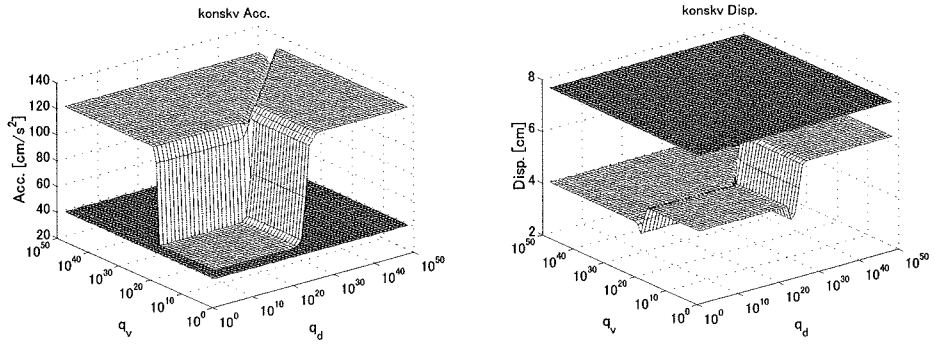

(a) Maximum response accelerations (b) Maximum relative displacement

Figure 23. Maximum response results (JMA NS)

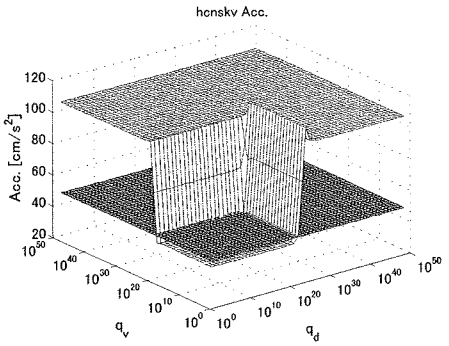

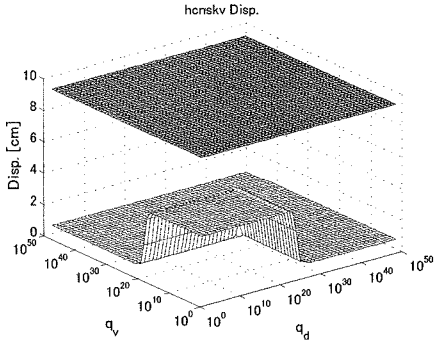

(a) Maximum response accelerations (b) Maximum relative displacement

Figure 24. Maximum response results (Hachinohe NS)

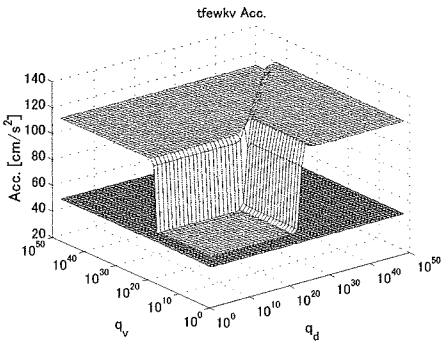

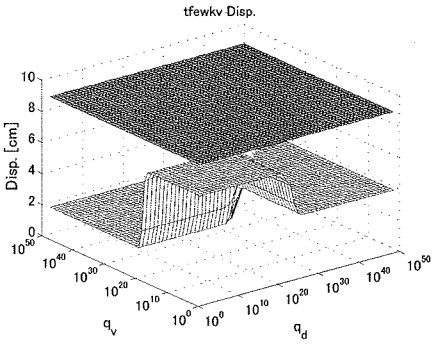

(a) Maximum response accelerations (b) Maximum relative displacement

Figure 25. Maximum response results (Taft EW)

The results show that the displacement reduction performance improved using semi-active seismic isolation for all weighting coefficients q_v and q_d, compared with the passive seismic isolation. However, the seismic isolation effects did not improve much more than the passive seismic isolations according to seismic waves. By comparing with the passive seismic isolation results, the weighting coefficients were selected in the following cases:

1) The relative displacement is almost in the same level and the response acceleration is smaller. (acceleration reduction)
2) Both the response acceleration and relative displacement are smaller. (acceleration and displacement reduction)
3) The response acceleration is almost in the same level and the relative displacement is smaller. (displacement reduction)

Figures 26, 27, 28 and 29 show the results of the analyses by these weighting coefficients

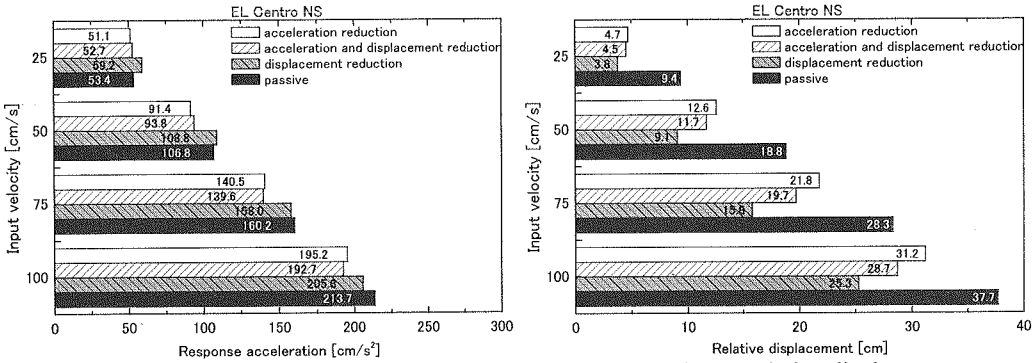

(a) Maximum response accelerations (b) Maximum relative displacement

Figure 26. Response results by selected weighting coefficients (EL Centro NS)

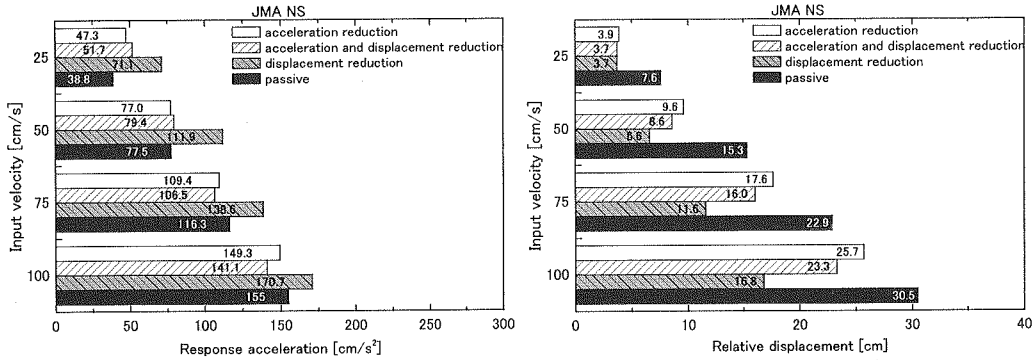

(a) Maximum response accelerations (b) Maximum relative displacement

Figure 27. Response results by selected weighting coefficients (JMA NS)

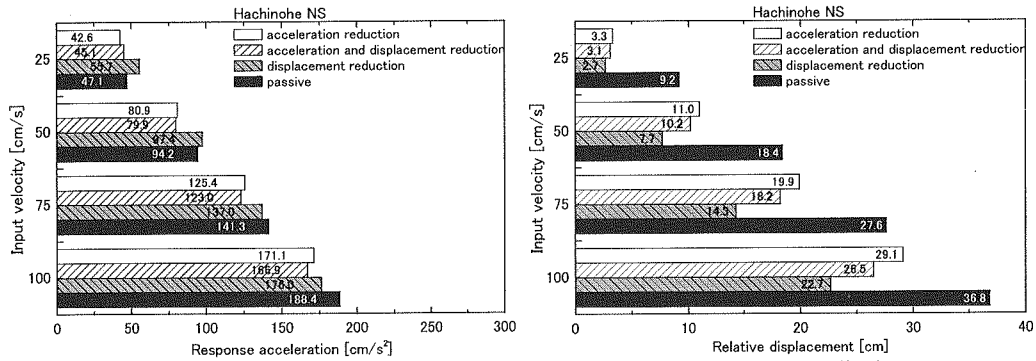

(a) Maximum response accelerations (b) Maximum relative displacement

Figure 28. Response results by selected weighting coefficients (Hachinohe NS)

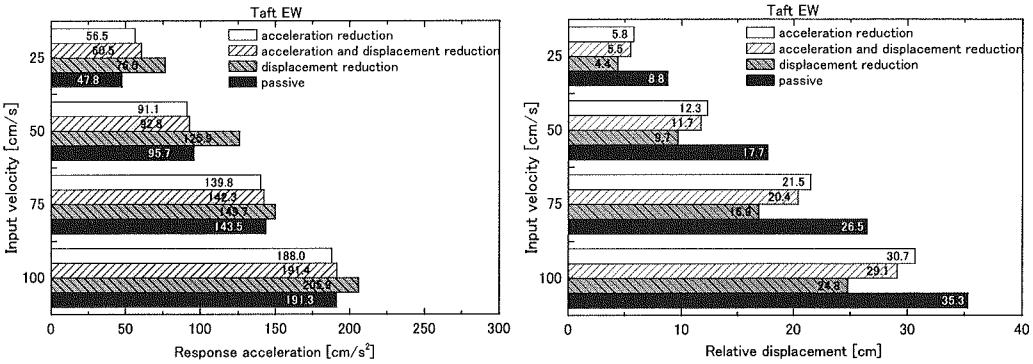

(a) Maximum response accelerations (b) Maximum relative displacement

Figure 29. Response results by selected weighting coefficients (Taft EW)

CONCLUSIONS

It was experimentally confirmed that the friction force of the releasing type controllable friction damper can be changed by controlling the piezoelectric actuator force.

Moreover, numerical model of the releasing type controllable friction damper was developed from the results of the characterization experiment. Then, the response analysis of the semi-active seismic isolation system designed from LQ and IOC using the numerical model laws was conducted. As a result, the seismic isolation effects and the relative displacement reduction effects of semi-active seismic isolation system using the controllable friction damper improved in comparison with the passive seismic isolation system.

REFERENCES

Fujita, T. (1991a) "Research, development and application of seismic isolation systems in Japan, Proceeding of the International Meeting on Earthquake Protection of Builgings" Ancona, Italy,6-8, June, 77/C-90/C.

Fujita, T., Kabeya, K., Hayamizu, Y., Aizawa, S., Higashino, M., Kubo, T., Haniuda, N., and Mori, T., (1991b). "Semi-active seismic isolation system using controllable friction damper (1st report, Development of controllable friction damper and fundamental study of semi-active control system)" Trans. of Japan Soc. Mech. Eng. , 57, 536 Ser.C, 1122-1128 (in Japanese).

Fujita, T., Shimazaki, M., Hayamizu, Y., Aizawa, S., Higashino, M., Kubo, T., and Haniuda, N. (1992) "Semi-active seismic isolation system using controllable friction damper (2nd report, Study of the system with distributed controllable friction dampers)" Trans. of Japan Soc. Mech. Eng. , 58, 551 Ser.C, 2012-2016 (in Japanese).

Shimazaki, M., and Fujita, T. (1996) "Experimental Study of Piezoelectric Actuator for Large-Scale Smart Structure (2nd Report, Actuator Characteristics of 25x25x36 Piezoelectric Actuator of Stack Type)" SEISAN-KENKYU Vol. 48, No. 9, 449-452 (in Japanese)

Yang, J.N., Akbarpour, A., and Ghaemmaghami, P., New optimal control algorithms for structural control, Journal of Engineering Mechanics, ASCE, 1987 Vol.133 No. 9, 1369-1386.